


The catalytic domain of free or ligand bound histone deacetylase 4 occurs in solution predominantly in closed conformation

Markus Schweipert¹ | Thomas Nehls² | Anton Frühauf¹ | Cecilé Debarnot¹ | Adarsh Kumar³ | Stefan Knapp³ | Frederik Lermyte² | Franz-Josef Meyer-Almes¹ 

¹Department of Chemical Engineering and Biotechnology, University of Applied Sciences, Darmstadt, Germany

²Department of Chemistry, Clemens-Schöpf-Institute of Chemistry and Biochemistry, Technical University of Darmstadt, Darmstadt, Germany

³Fachbereich Biochemie, Chemie und Pharmazie, Institut für Pharmazeutische Chemie, Goethe-University Frankfurt, Frankfurt Am Main, Germany

Correspondence

Franz-Josef Meyer-Almes, Department of Chemical Engineering and Biotechnology, University of Applied Sciences, 64295 Darmstadt, Germany.

Email: franz-josef.meyer-almes@h-da.de

Funding information

Deutsche Forschungsgemeinschaft; State of Hesse

Review Editor: Carol Beth Post

Abstract

Human histone deacetylase 4 (HDAC4) is a key epigenetic regulator involved in a number of important cellular processes. This makes HDAC4 a promising target for the treatment of several cancers and neurodegenerative diseases, in particular Huntington's disease. HDAC4 is highly regulated by phosphorylation and oxidation, which determine its nuclear or cytosolic localization, and exerts its function through multiple interactions with other proteins, forming multiprotein complexes of varying composition. The catalytic domain of HDAC4 is known to interact with the SMRT/NCOR corepressor complex when the structural zinc-binding domain (sZBD) is intact and forms a closed conformation. Crystal structures of the HDAC4 catalytic domain have been reported showing an open conformation of HDAC4 when bound to certain ligands. Here, we investigated the relevance of this HDAC4 conformation under physiological conditions in solution. We show that proper zinc chelation in the sZBD is essential for enzyme function. Loss of the structural zinc ion not only leads to a massive decrease in enzyme activity, but it also has serious consequences for the overall structural integrity and stability of the protein. However, the Zn²⁺ free HDAC4 structure in solution is incompatible with the open conformation. In solution, the open conformation of HDAC4 was also not observed in the presence of a variety of structurally divergent ligands. This suggests that the open conformation of HDAC4 cannot be induced in solution, and therefore cannot be exploited for the development of HDAC4-specific inhibitors.

KEYWORDS

allosteric regulation, conformation sensitive mass spectrometry, conformational, conformational equilibrium, conformations, HDAC4, ligand binding, NMR, transient binding pockets

This is an open access article under the terms of the [Creative Commons Attribution-NonCommercial-NoDerivs](https://creativecommons.org/licenses/by-nc-nd/4.0/) License, which permits use and distribution in any medium, provided the original work is properly cited, the use is non-commercial and no modifications or adaptations are made.

© 2024 The Authors. *Protein Science* published by Wiley Periodicals LLC on behalf of The Protein Society.

1 | INTRODUCTION

To ensure survival, cells must adapt to changes in their surrounding environment and within their cytosol. One mechanism of adaptation involves posttranslational modifications such as phosphorylation, ubiquitination, and deacetylation (Bradley, 2022). Histone deacetylases (HDACs) are enzymes that catalyze the removal of acetyl groups from lysine residues on histone proteins, a process that plays a crucial role in gene expression and epigenetic regulation. In the past three decades, HDACs have emerged as promising drug targets for the treatment of cancer and neurodegenerative diseases. Currently, there are five approved drugs (Vorinostat [Zolinza[®]], Panobinostat [Farydak[®]], Belinostat [Beleodaq[®]], Romidepsin [Istodax[®]], and Tucidinostat [Epidaza[®]]) that target HDACs (Bondarev et al., 2021; Ho et al., 2020). There are a total of 18 known mammalian HDACs, which are categorized into four classes based on their homology and gene sequence. Class II is further divided into two subclasses, IIa and IIb. Classes I, II, and IV are zinc-dependent, while class III consists of NAD⁺-dependent enzymes (Witt et al., 2009). Class IIa HDACs exhibit unique features compared with the other HDAC classes. They have a C-terminal deacetylation domain, a sequence for nuclear export, as well as an N-terminal myocyte enhancer factor 2 (MEF2) domain (Shen et al., 2023). HDAC4, belonging to Class IIa, is one of the largest isozymes in the HDAC family, with an approximate molecular weight of 120 kDa and a length ranging from 972 to 1084 amino acids depending on splicing. It is primarily expressed in the heart, brain, and skeletal muscle, where it plays a key role in tissue growth and physiological development (Asfaha et al., 2019; Wang, Qin, & Zhao, 2014). Like all Class IIa HDACs, HDAC4 has a second bound zinc ion in a highly flexible structural zinc binding domain (sZBD; Bottomley et al., 2008). This zinc ion connects two protein segments that otherwise would distort the globular protein structure: One segment is a 17 amino acid loop ($\alpha 1-\alpha 2$) containing three zinc chelating residues (His665, Cys667, and His678). The other segment is a helix-turn-helix motif of 35 amino acids ($\alpha 6-\alpha 7-\beta 3-\beta 4$) followed by a β -hairpin with a fourth zinc chelating residue (Cys751). These residues are highly conserved across all Class IIa HDACs and absent in other HDACs (Bottomley et al., 2008). In vivo HDAC4 facilitates the active transport of HDAC3 between the nucleus and the cytoplasm through a multiprotein complex involving nuclear receptor corepressor (NCoR) and silencing mediator for retinoid or thyroid hormone receptors (SMRT; Fischle et al., 2001; Wang, Qin, & Zhao, 2014). HDAC4 itself exhibits low to no enzymatic activity for acetylated substrates, and there is no known in vivo substrate (Ho et al., 2020). HDAC4 is implicated

in nephrological and neurodegenerative diseases, as well as various cancer types, including breast cancer (Clocchiatti et al., 2011; Mielcarek et al., 2015; Wang, Liu, et al., 2014; Wang, Qin, & Zhao, 2014; Witt et al., 2009). Furthermore, previous studies have demonstrated that reducing the in vivo activity of HDAC4 in animal models alleviates symptoms of Huntington's disease, offering a potential strategy for the treatment of this currently incurable condition (Federspiel et al., 2019; Mielcarek et al., 2013). In this study, we expressed the C-terminal domain of human HDAC4, comprising of amino acids Thr648 to Thr1057. This domain includes both the catalytic domain and the sZBD.

Currently, 12 structures of HDAC4 and 5 structures of the highly similar HDAC7 have been deposited in the Protein Data Bank (PDB). In the case of HDAC4 (PDB-ID: 4CBY) and HDAC7 (PDB-ID:3ZNS) superposition of the catalytic domains (10 Å radius of the catalytic zinc ion) revealed a root mean square deviation (RMSD)-value of 0.293 Å. Most HDAC4 and HDAC7 structures represent the closed conformation in the presence or absence of ligands. Only two structures (PDB-ID's 2VQM and 2VQJ), reported by Bottomley et al., display a crystal structure in the so-called open conformation, where the sZBD is flipped out of the globular protein structure, resulting in a significant conformational rearrangement of the catalytic domain (Mielcarek et al., 2013). The two structures of the open conformation were solved in the presence of TFG ligand (2,2,2-trifluoro-1-(5-[(3-phenyl-5,6-dihydroimidazol[1,2-A]pyrazin-7(8H)-YL)carbonyl]thiophen-2-YL)ethane-1,1-diol)(PDB-ID: 2VQJ) and its hydroxamic acid analogue (PDB-ID: 2VQM) and they have been refined at a resolution of 2.1 and 1.8 Å, respectively.

According to this report, the open conformation was induced to prevent clashes between the ligand and the sZBD of HDAC4. Moreover, mechanistic considerations of ligand binding to interconverting conformations of HDAC4 have shown that even ligands with higher affinity for the HDAC4's open conformation may eventually bind to its closed conformation because of the energetically favored closed apo-conformation in equilibrium (Schweipert et al., 2021). Bottomley et al. also demonstrated a change in the zinc chelating residues between the open and closed conformation. In the ligand-bound open conformation, the chelators of the structural zinc ion change to His665 and His678, whereas in the native closed conformation, they are Cys669 and His675, respectively. Additionally, the authors created a double mutant variant (Cys669Ala/His675Ala) to disrupt the sZBD. The authors performed immunoprecipitation and Western Blotting experiments, which demonstrated that the variant, in comparison to HDAC4's wild type, failed to bind the SMRT/NCoR repressor complex. These findings

suggested that the closed conformation was the biologically relevant conformation, as a properly ordered sZBD is crucial for the formation of multiprotein complexes. However, the crystal structure of the double mutation variant was not solved.

We hypothesized that if the open conformation would be populated in solution, it could be exploited for designing inhibitors that specifically target this unique conformation as a viable strategy to solve the general isozyme selectivity issue of HDAC inhibitors (Di Giorgio et al., 2015; Yang et al., 2019). In this study, we aimed to elucidate, whether the open conformation of HDAC4 can be detected in solution under physiological conditions. Therefore, we analyzed the open crystal structure of HDAC4 and also conducted molecular docking of the TFG ligand into the closed conformation of HDAC4 to identify the particular amino acids causing proposed steric clashes that may result in the reported open conformation. For measurements of apo-HDAC4 and HDAC4 in complex with the TFG ligand in solution, we employed ^{19}F -NMR. Additionally, we utilized conformation-sensitive ion mobility-mass spectrometry (IM-MS) to investigate conformational changes in apo-HDAC4 and HDAC4 bound to the TFG ligand, as well as various common HDAC ligands. Furthermore, we evaluated the integrity of the double mutant variant through enzyme

activity, thermal stabilization, IM-MS, and circular dichroism (CD)-spectroscopy.

2 | RESULTS AND DISCUSSION

2.1 | Crystal structures suggest two different major conformations of HDAC4

Our comparison between the two HDAC4 conformations was based on the x-ray structures of the open and closed conformation (PDB-IDs 2VQJ and 4CBY, respectively). We chose the 4CBY structure to represent the closed conformation instead of 2VQW (solved by Bottomley and colleagues) because 4CBY provided a better resolution of the HDAC4 wild-type structure, whereas 2VQW was a gain-of-function variant (H976Y) with lower resolution (Bottomley et al., 2008; Burli et al., 2013). When superposing the 4CBY and 2VQW crystal, it was evident that both backbones were essentially identical (RMSD-value of 0.3 Å). Upon superimposing the x-ray structures of the open and closed conformations and plotting the RMSD values against the respective residue numbers, two regions stood out: residues 23–33 and residues 89–125. These regions represent the central loop and helix in the sZBD, respectively (Figure 1). Apart from these two

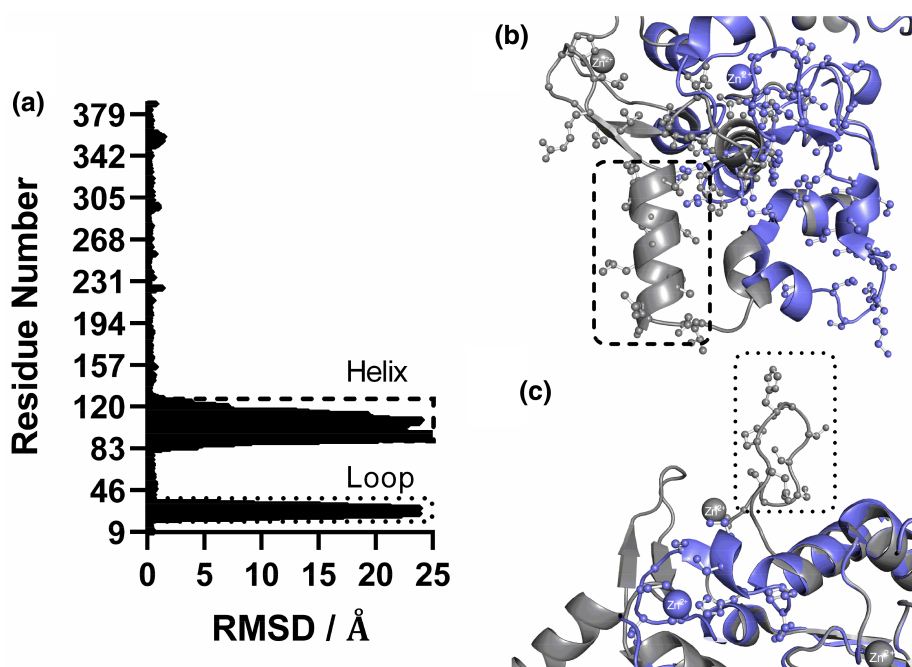


FIGURE 1 Superimposition root mean square deviation (RMSD) plot of the open and closed reported crystal structures of human histone deacetylase 4 (HDAC4) and comparison between helix and loop regions of the structural zinc-binding domain (sZBD).

(a) Superposition RMSD plot of x-ray structures: open conformation (PDB-ID: 2VQJ) and closed conformation (PDB-ID: 4CBY), revealed two regions with high structural diversity (loop region: dotted cycle; helix region: dashed cycle). Close up the differences in the (b) helix and (c) loop region of the sZBD between the open (gray) and the closed (blue) conformation of HDAC4. Residues 150–380 were used for superposition before RMSD calculation.

regions, the remaining backbone conformations are very similar, with RMSD values of ~ 5 Å or less with regard to their C α atoms. In the NMR experiment described below, we utilized the expected substantial conformational changes in one of these regions to elucidate, whether the open conformation exists in solution or if it is solely observed in the reported crystal structures.

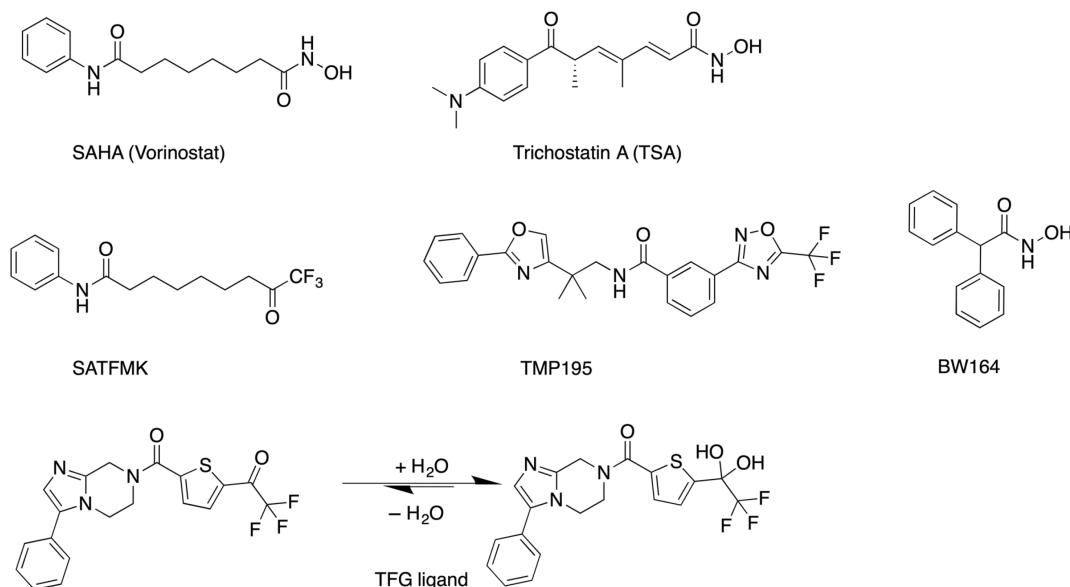
2.2 | Potential influence of crystal packing effects on structures of the open conformation of HDAC4

To convince ourselves that the open conformation of HDAC4 was not a tracing error, we obtained the structure factor file of the HDAC4 open conformation crystal (PDB-ID: 2VQJ) and used a newer, higher-resolution template (PDB-ID: 5ZOO) for molecular replacement. The search model was in the closed conformation. We successfully traced a path that was mostly similar to PDB-ID: 2VQJ (Figure S1), although there were slight differences in the loop regions, some of which exhibited a lack of electron density. However, crystal contacts appeared to have an influence on backbone conformation. Upon comparing the packing, it appeared that both loop1 (Lys664 to Ala679) and loop2 (Leu728 to Ser767), adopted an open conformation in the reevaluated structural model and PDB-ID 2VQJ (Figure S2A). It is conceivable that crystal packing may play a role, as the space occupied by the loops (PDB-ID: 5ZOP) seemed to be

occupied by symmetry molecules (Figure S2B,C). Similar trends were observed in other structures such as PDB-IDs 5A2S and 4CBY comparing both loop conformations. Structures such as PDB-IDs 6FYZ and 4CBT showed a disordered loop2, and the corresponding region lacked electron density. In summary, it seems that loop2 exhibits mobility. The opening of loop2 may also contribute to the opening of loop1 by pushing it away and occupying its position (Figure S2D). Thus, it seems possible that the “open” conformation of HDAC4 was the result of crystal packing.

2.3 | Ligands can adopt beneficial binding poses in the closed conformation of HDAC4

The observation that some inhibitors bound to the open conformation of HDAC4 in crystal structures was attributed to possible steric interference of inhibitors with the closed conformation. We performed flexible docking of the TFG ligand (Scheme 1), which was crystallized in the open conformation of HDAC4 (PDB-ID: 2VQJ), into the binding pocket of the closed conformation of HDAC4 (PDB-ID: 4CBY) in order to look for possible steric clashes between the ligand and HDAC4. Docking resulted in a binding pose with strong metal binding by the hydrated trifluoromethyl warhead and additional conventional hydrogen bonds between the TFG ligand and His802 as well as His803 (Figure 2). The hydrophobic



SCHEME 1 Ligands used in this study. For the TFG ligand the equilibrium between its trifluoromethyl and geminal diol moiety is shown.

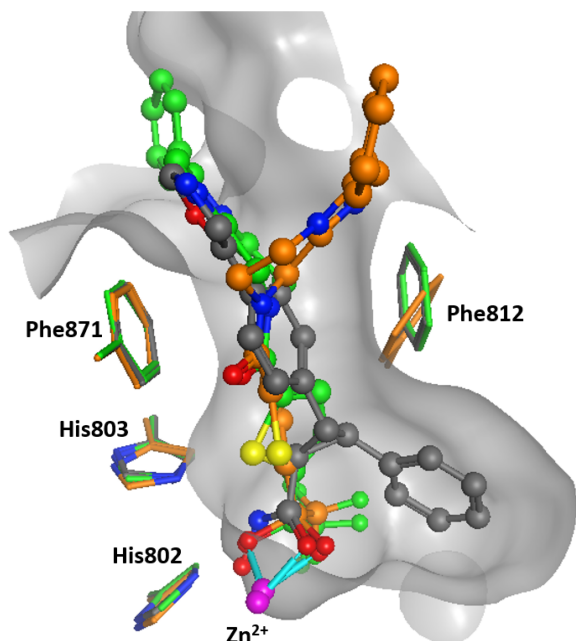


FIGURE 2 Docking pose of TFG ligand within the binding pocket of the closed conformation of Human histone deacetylase 4 (HDAC4; PDB-ID: 4CBY). HDAC4 in complex with cocrystallized hydroxamic acid ligand is colored dark gray, the docked complex of HDAC4 and TFG ligand is shown in green, and the superposed complex with crystallized TFG-ligand (PDB-ID: 2VQJ) is orange. The catalytic zinc ion is colored magenta. The metal bonds between the hydroxamate and the hydrated trifluoromethyl warhead of bound ligands are shown as cyan lines. The trifluoromethyl warhead of the TFG ligand is displayed in its geminal diol form as present in solution (see Scheme 1).

central aromatic moiety of the docked TFG ligand was sandwiched between opposite Phe812 and Phe871, which define the narrow hydrophobic binding channel of the closed conformation. The docking score of the TFG ligand (-14.6) was even better than that for the cocrystallized hydroxamate ligand (-12.0 ; Table S3). For comparison, the IC_{50} -value for latter ligand against the catalytic domain of HDAC4 was determined to be 20 nM (Burli et al., 2013). We observed neither steric clashes, nor did the ligand induce significant conformational changes in order to efficiently bind to the active site pocket. The docked and crystallized TFG ligands show very similar Zn^{2+} binding, but differ in the distant phenyl-imidazol-dihydropyrazine cap group. The cap groups in both binding poses project into free solution, but in different directions. However, none of the binding poses causes clashes with the closed conformation of HDAC4 (PDB-ID: 4CBY). Based on these docking results, there was no obvious reason why HDAC4 should be forced to open the closed conformation to enable binding of the TFG ligand.

2.4 | Chelation of zinc ion in sZBD determines the structural and functional integrity of the entire HDAC4 enzyme

Bottomley et al. (2008) introduced an HDAC4 variant in which two amino acid residues, which coordinate the zinc ion in the sZBD of the wild-type protein, were mutated (Cys669Ala and His675Ala). To elucidate the structural function of these amino acids, we expressed and purified a double exchange mutant variant and compared its biochemical and biophysical attributes to those of wild-type HDAC4. We discovered drastic differences in enzyme yield, enzyme activity, thermal stabilization by ligands, and structural composition between the two variants. The yields of the wild type and the variant were 11.4 and 0.3 mg/L, respectively, which implies a 38-fold decrease in yield compared with the wild type (Figure 3a). As mentioned earlier, HDAC4 displays minimal enzymatic activity towards simple acetylated substrates. However, it exhibits significant activity for trifluoroacetylated substrates. Taking advantage of this, we conducted an analysis of enzyme activity for both the wild type and the double mutant variant, revealing significant differences between the two enzymes. The wild type converted $5.95 \pm 0.17 \mu\text{M/h nM}^{-1}$ substrate. In agreement with Bottomley et al., we determined drastically reduced enzymatic activity ($0.020 \pm 0.002 \mu\text{M/h nM}^{-1}$) of the double mutant variant. This equaled an enzyme activity loss of about 300-fold (Figure 3b). This study confirmed the importance of the sZBD for substrate recognition, as proposed by Bottomley et al. With a structurally disturbed sZBD HDAC4 was essentially not able to convert substrate. The melting point of the wild type ($54.6 \pm 0.1^\circ\text{C}$) and the variant ($53.5 \pm 0.1^\circ\text{C}$) were similar, with a decrease in thermal stability by 1.1°C of the double mutant variant. However, upon closer examination of the raw thermal stability data, we observed that the double mutant variant displayed a 4.6-fold smaller measurement window between the base and peak of the melting curve (Figure 3c). Furthermore, the base of the variant's melting curve was notably higher compared with the wild type. A significantly higher baseline in the assay strongly indicates that the protein's surface is more hydrophobic (e.g., unfolded/denatured) compared with a protein with a low baseline, as was observed in this case (please refer to the Thermal Shift method in the experimental section for further explanation). The similar melting points are interesting because typically, an unfolded or denatured protein would exhibit lower thermal stability, which was not observed here. The increased hydrophobicity is an indicator for overall protein unfolding, perhaps attributed to a distorted or unfolded sZBD or as

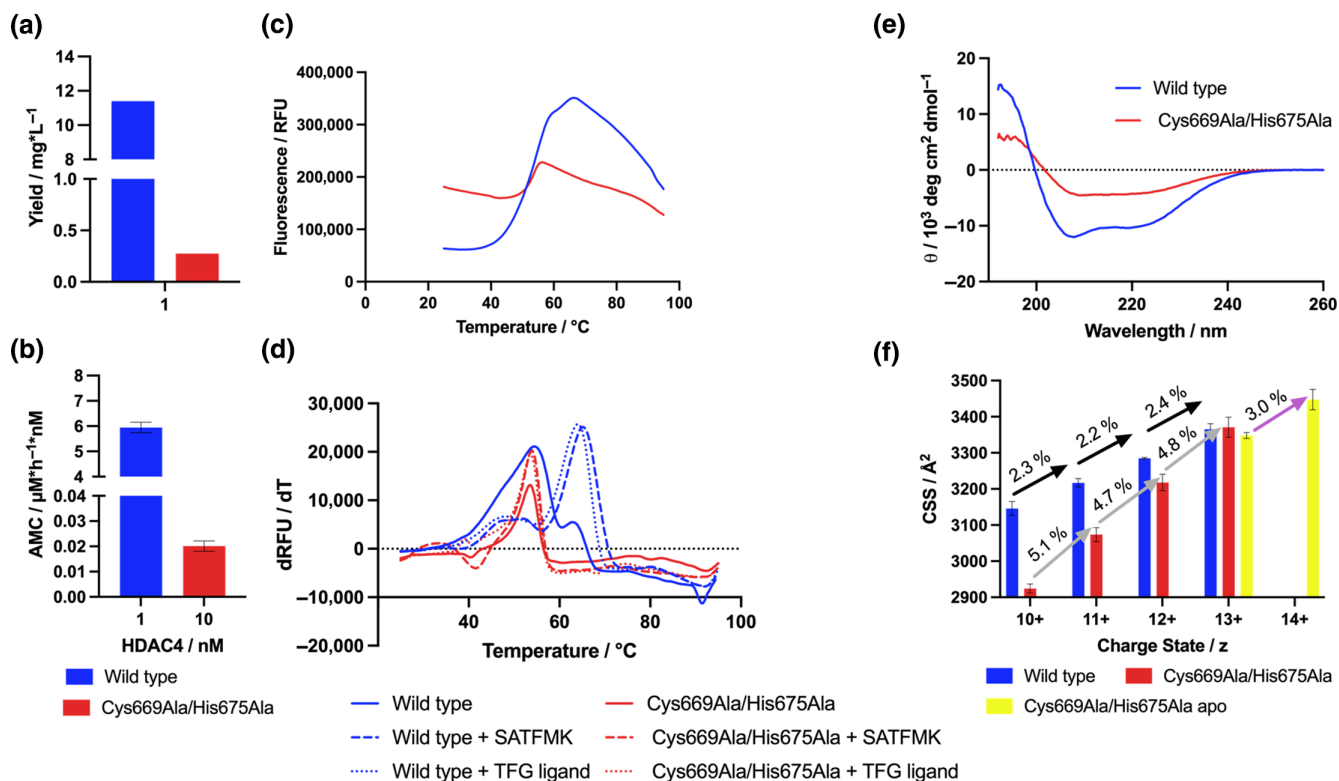


FIGURE 3 Biophysical and biochemical comparison between human histone deacetylase 4 (HDAC4) wild type and the Cys669Ala/His675Ala variant with the double mutation located in the structural zinc-binding domain (sZBD). (a) Yield of recombinant protein production. (b) Enzyme activity normed to respective HDAC4 concentrations. Enzyme activity assays were performed in triplicate; error bars are displayed as standard deviation. (c) Thermal stability. (d) Thermal stabilization of HDAC4 wild type and the Cys669Ala/His675Ala variant in the presence of SATFMK and TFG ligand. Thermal stability assays were performed in quadruples. Plotted are means without error bars for the sake of better clarity. Figures including error bars are provided in Figure S5 and S6. (e) Circular dichroism (CD) spectra in the range between 192 nm to 260 nm. CD-spectra are displayed as the means of 10 scans. (f) Ion mobility-mass spectrometry (IM-MS) data of HDAC4 wild type, HDAC4 Cys669Ala/His675Ala variant with one missing zinc ion and HDAC4 Cys669Ala/His675Ala (apo) with two missing zinc ions. Measurements were performed in triplicate; error bars are displayed as standard deviation. Black, gray, and purple arrows indicate average collision cross section (CCS)-value increases as a function of charge z of the wild type, Cys669Ala/His675Ala variant, and Cys669Ala/His675Ala variant (apo), respectively. 1D-MS spectra of the charge states are provided in Figure S16.

a consequence thereof. Furthermore, we observed a loss of ligand binding to the double mutant variant, which is another indicator for significant misfolding of the enzyme. The TFG ligand and SATFMK stabilized HDAC4 wild type by 9.45 ± 0.04 and $10.71 \pm 0.05^\circ\text{C}$, respectively. Contrary, the same ligands exhibited way less stabilization regarding the Cys669Ala/His675Ala double mutation variant, with values of 0.26 ± 0.05 and $0.39 \pm 0.02^\circ\text{C}$ (Figure 3d). The CD-spectra data of HDAC4 wild type and the double mutant variant revealed severe changes in secondary structure composition of the two enzymes. Based on the CD-spectra, the wild-type HDAC4 displayed a characteristic pattern indicative of a protein primarily composed of more helices than β -sheets (Greenfield, 2006). Conversely, the double mutant variant exhibited less pronounced secondary structures and seemed to be dominated by β -sheets instead of helices (Figure 3e). Fitting the CD-spectra data

confirmed the initial assumption of significant shifts in structural composition (Table 1). The drastic shift in structural composition between the two enzymes was apparently caused by the two mutations in the sZBD considering this is the only difference between these two proteins. Moreover, IM-MS measurements of HDAC4 wild type and the Cys669Ala/His675Ala double mutation variant revealed that the variant contained only one zinc ion (Figure 3f). The lost zinc ion was most likely the one located in the sZBD, because this region was disturbed by the mutations and these residues coordinate the structural zinc ion in HDAC4's closed conformation. In addition, the missing zinc ion was unlikely to be the catalytic zinc ion because we determined very low but significant residual enzyme activity of this variant (Figure 3b). The HDAC4 double mutant variant exhibited by far the smallest collision cross section (CCS)-value in charge states $z = 10+$, $z = 11+$, and $z = 12+$ compared with the wild

TABLE 1 Structural composition of HDAC4 wild type and the Cys669Ala/His675Ala double mutant variant derived from CD-spectra data.

	Wild type	Cys669Ala/His675Ala
Helix/%	22.6	6.7
β -Sheets/%	17.7	31
Turns/%	14.1	15
Other/%	45.6	47.3

Abbreviations: CD, circular dichroism; HDAC4, human histone deacetylase 4.

type. This indicated that the protein became more compact upon gas phase collapse and, at lower charge states, adopted a smaller collision cross section (CCS) value than the wild type, which is consistent with this variant having larger segments without folded secondary structures (Breuker & McLafferty, 2008). Furthermore, the significant increase in CCS values of the HDAC4 double mutant variant with increasing charge state demonstrated that the intramolecular interactions of its secondary structures were considerably weaker overall compared with the wild type. As a result, the variant was less resistant to Coulomb repulsion, leading to more pronounced unfolding and subsequently higher CCS values. For further explanations, please refer to the respective IM-MS method in the experimental section. However, CCS values alone only represent the overall folding state of the entire protein and do not provide any information about the unfolding of individual domains. Nevertheless, considering the difference compared with the wild type, massive disruption and at least partial unfolding of the double mutant variant can be expected. Additionally, at higher charge states of $z = 13+$ and $14+$, we measured not only the HDAC4 double mutant variant with one missing zinc ion but also the variant without any bound zinc ions (Cys669Ala/His675Ala apo; Figure 3f). This suggested that in this variant not only the sZBD was disturbed, but the whole intrinsic stability was impaired to the extent that, at higher charge states, even the catalytic zinc ion cannot be securely bound. In comparison, the wild type did not lose any of its zinc ions at higher charge states, not even the structural zinc ion. This finding was intriguing because one might expect, given that the chelators of the structural zinc ion change between the open and closed conformations of HDAC4 (according to the respective crystal structures), that the zinc ion in the sZBD would be bound less tightly. This inconsistency may also suggest that the structure observed in the crystal of the open conformation does not accurately represent the conformation in solution. However, it is known that the metal ions in HDACs are not bound tightly to the

protein, which is normal for metalloenzymes (Mirts et al., 2019). There have been reports of HDACs's catalytic zinc ion being exchanged with other metal ions, such as cobalt or iron, which is not only the case in vitro but also in vivo (Dowling et al., 2010; Gantt et al., 2006). These findings indicate the double mutant variant is in a highly disturbed conformational state.

In one of our previous works, we discussed the possible importance of the salt bridge formed by Glu764 and Arg730, which is located in the sZBD. We demonstrated that an HDAC4 Glu764Ala variant has impaired ligand recognition, possible due to structural effects in the sZBD (Schweipert et al., 2021). The applied methodologies in this study, except for metal binding, do not provide insights into the specific causes of the highly disturbed conformational state of the double mutant variant. However, it appears plausible that the mentioned salt bridge might also be impaired or even broken in a severely disturbed sZBD. The findings in this study imply that the double mutant variant is highly disrupted to the extent that it impairs protein synthesis, behavior, and structural composition, leading to the mentioned consequences. Our data suggested that the results of the immunoprecipitation experiments revealing that HDAC4 was not able to participate in its designated protein-protein interaction by Bottomley et al. cannot be solely contributed to a disturbed sZBD. The disturbance introduced by these mutants was likely so severe that the protein was at least partially unfolded to an extent that it lost most of its structural features.

2.5 | Ligands bind exclusively to the closed conformation of HDAC4 under physiological conditions

Using IMPACT software, theoretical CCS values can be calculated for the drift gas helium based on crystal structures (Marklund et al., 2015). The actual measurements were performed using nitrogen as drift gas. We explain the difference in drift gases (including a helium-nitrogen regression) in the respective IM-MS method in the experimental section. With x-ray structures representing the closed (PDB-ID: 4C8Y) and open (PDB-ID: 2VQJ) conformation, theoretical CCS values were calculated using the trajectory method and compared with actual measurements (Figure 4). The measured CCS values at charge state $z = 10+$ for apo HDAC4, HDAC4 in complex with either the TFG ligand or BW164, and the simulated CCS values based on the x-ray structure of HDAC4's closed conformation were highly similar. These findings were surprising because, based on the simulation results utilizing the x-ray structures, we expected a significant

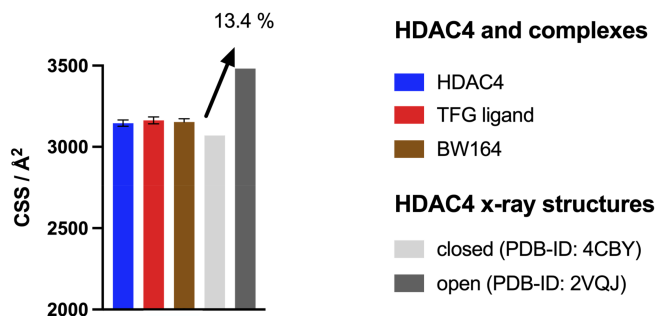


FIGURE 4 Comparison between measured collision cross section (CCS) values and simulations based on x-ray structures. Colored bars indicate measured CCS values of free human histone deacetylase 4 (HDAC4) and HDAC4 in complex with respective ligands ($z = 10+$). Gray bars indicate CCS values calculated with IMPACT software for the closed (PDB-ID: 4CBY) and open (PDB-ID: 2VQJ) conformation of HDAC4 utilizing the trajectory method (TJM). Black arrow and percentage indicate increase of simulated CCS values between open and closed conformation. Simulated values were computed using helium as drift gas.

increase in CCS values between ligand-free HDAC4 and HDAC4 in complex with the TFG ligand (open conformation). Consequently, we concluded that the x-ray structure of the open conformation was unlikely to represent HDAC4 in complex with the TFG ligand in solution. Additionally, there is a reported structure of an analogue of ligand BW164 bound to HDAC4 in its closed conformation (PDB-ID: 6FYZ), further emphasizing that both apo-HDAC4 and the tested complexes predominantly adopt the closed conformation.

In addition to the already discussed samples we also tested various known HDAC inhibitors (Scheme 1) in complex with HDAC4 to determine whether they induce conformational changes. However, all samples exhibited similar CCS values (Figure 5). While one could argue that, on average, the complexes displayed slightly larger CCS values compared with apo HDAC4, these differences fall within the margin of error and are not statistically significant, indicating that all measured complexes adopt the closed conformation or minor variations thereof. Furthermore, the complexes exhibited slow and steady increases in CCS values with increasing charge state, indicating the structural stability of the complexes. We already discussed the contrasting behavior of low-stability samples in the previous chapter. The findings suggest that neither the TFG ligand nor any other tested ligand induced a significant conformational change upon binding to the enzyme. HDAC4 bound to the TFG ligand showed a CCS-value of 3162 \AA^2 at a charge state of $z = 10+$. This value is 9.2% smaller when compared with the simulations with helium as the drift gas and 19% smaller compared with simulations with nitrogen as the

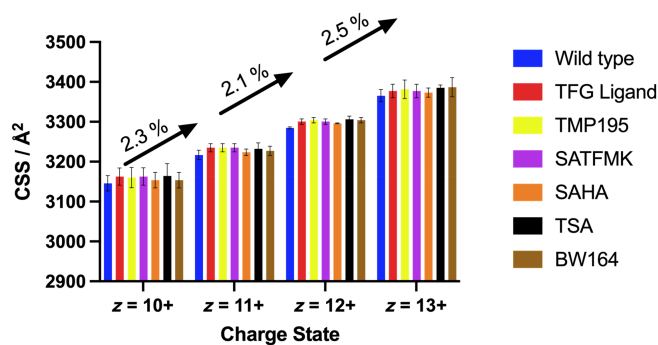


FIGURE 5 Change of collision cross section (CCS) during ion mobility-mass spectrometry measurements. Displayed are CCS values of free human histone deacetylase 4 (HDAC4) wild type (blue) and the wild type in complex with respective ligands. Black arrows indicate average CCS-increase of HDAC4 and HDAC4 in complex with different ligands with higher charge state. Measurements were performed in triplicate; error bars displayed as standard deviation.

drift gas. Moreover, the actually measured difference between HDAC4 in complex with the TFG ligand and apo HDAC4 was only 0.54%. This also provided compelling evidence that the x-ray structure of HDAC4's open conformation (PDB-ID: 2VQJ) is unlikely to represent its actual conformation when bound to the TFG ligand in solution under native conditions. For contextual reference, HDAC4 wild type in its closed conformation exhibited 2.5% and 9.7% differences between the actual measurements and simulated CCS-value using helium as drift gas and the corrected simulated CCS values using nitrogen-helium regression, respectively, which is a typical error between the simulation and the measured values (Turzo et al., 2023). This, and the data from Figure 4, suggests that the closed conformation in the x-ray structure represents more closely the enzyme's actual conformation.

Further validation was performed via NMR by observing the ^{19}F chemical shift of a site-specific incorporated 4-trifluoromethylphenylalanine (tfmF) in the presence and absence of the TFG ligand (Scheme 1). ^{19}F NMR coupled with amber codon suppression labeling is a powerful tool to study proteins and is often used in conformational studies (Chen et al., 2013; Gronenborn, 2022). Amber codon suppression enables a site-selective incorporation of a non-canonical amino acid (ncAA) containing a ^{19}F nucleus, which exhibits high sensitivity and a wide chemical shift range (Gronenborn, 2022; Kitevski-LeBlanc & Prosser, 2012). The chemical shift is highly responsive towards changes in the local conformational and electronic environment and varies between probes (Kitevski-LeBlanc & Prosser, 2012). Compared with other CF_3 probes the aryl- CF_3 moiety seems to be most

responsive towards changes in polarity (Ye et al., 2015). In particular, tfmF has been shown to be highly sensitive for subtle conformational changes induced by binding of substrates, inhibitors or cofactors (Jackson et al., 2007; Ye et al., 2015). Mass spectra of the two HDAC4 variants (Figure S13), 2D mobilogram with drift time and mass-to-charge ratio of HDAC4 wild type (Figure S14) as well as the mobilogram of the CCS plots (Figure S15) are provided in Supplementary material S1.

To identify suitable mutation sites, crystal structures of HDAC4 in the open (PDB-ID: 2VQJ) and closed (PDB-ID: 4CBY) conformation were superposed and amino acids located in the moving sZBD domain, experiencing a significant change in the local environment, were selected (Figure 6a). Out of the potential residues in the sZBD domain (Ser671 to Ser674, Lys736, Lys737, and Phe746), exhibiting transitions in the range of 14–23 Å, Phe746 displayed significant changes in the local environment. In the open conformation Phe746 is part of the sZBD helix region, facing the solvent and having mostly hydrophobic amino acids (Leu742, Val745, Val754, Val756, Leu661, His766, and Trp762) and certain polar

amino acids (Arg748 and Asp757) in its 5 Å proximity (Figure 6b). In the closed conformation Phe746 is located in a loop region, pointing into a small pocket with aromatic (Trp762, Tyr814, and Tyr723) hydrophobic (Val754, Val745, Val722, and Val756) and hydrophilic (Ser744) amino acids in its 5 Å proximity (Figure 6c). On the basis of this framework, we expected a strong difference in ^{19}F chemical shifts of tfm Phe746 in the open and closed conformation. To measure the chemical shift in the closed conformation, experiments were performed without ligand since the closed conformation is dominant in solution (see previous chapter). To favor the open conformation, we performed a second measurement in the presence of TFG ligand, which should bind to the open conformation, thus inducing a change in the local environment of Phe746, thereby resulting in a difference in chemical shift. Additionally, NMR measurements of native HDAC4 and the free nAA were collected as reference. The binding of the TFG ligand to HDAC4 in NMR buffer was confirmed via thermal shift. The ligand induced a thermal stabilization of $11.75 \pm 0.03^\circ\text{C}$, indicating strong binding in the used buffer system (Figure S7).

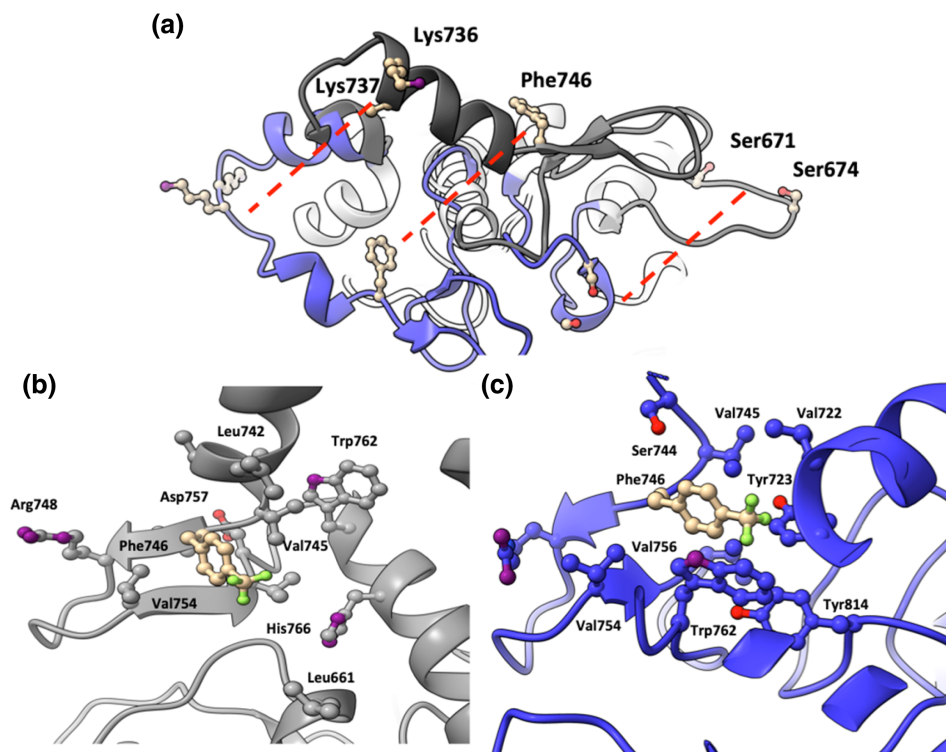


FIGURE 6 Potential mutation sites and changes in microenvironment. (a) Top view on superposed human histone deacetylase 4 (HDAC4) crystal structures in the open (gray, PDB-ID: 2VQJ) and closed (blue, PDB-ID: 4CBY) conformation with indicated amino acids as potential mutation sites and their transition paths indicated as red dashed lines. According to the x-ray structures Phe746 shows a transition of 20.4 Å between the respective C α atoms in the open and closed conformation. (b,c) Change in microenvironment of a modeled tfmPhe746 between the proposed open (b) and closed (c) conformation of HDAC4 with residues within 5 Å proximity. Nitrogen, oxygen, and fluorine atoms are colored purple, red and green, respectively. Distances between the CF $_3$ moiety and neighboring atoms of sidechains are indicated in Figure S17. Images were created using the UCSF ChimeraX visualization software (version ChimeraX-1.4; Goddard et al., 2018).

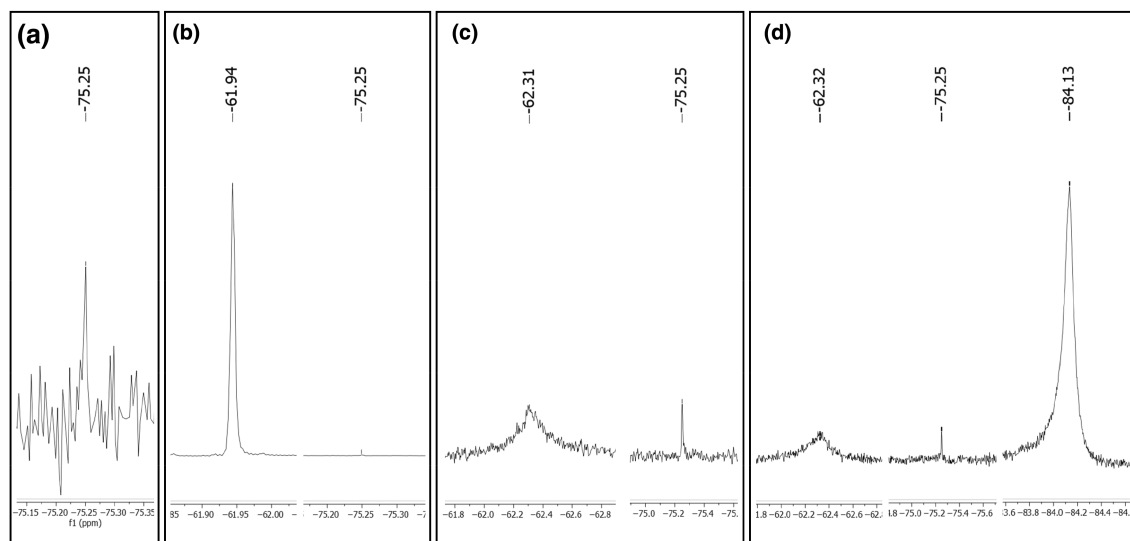


FIGURE 7 Clipped spectra of four NMR experiments. (a) Spectrum of unlabeled protein, (b) free amino acid (tfmPhe), (c) labeled protein, and (d) labeled protein in presence of the TFG ligand. Spectra were calibrated relative to the signal at -75.25 ppm. The full-recorded spectra were free of any additional signals (Figure S8).

As anticipated, the ^{19}F -NMR spectrum of unlabeled HDAC4 did not show a protein-related signal but a small signal at -75.25 ppm, which occurred in all samples and was used as reference (Figure 7a). The free nCAA displayed a distinct and sharp signal at -61.9 ppm (Figure 7b) and the incorporated nCAA exhibited a signal at -62.3 ppm (Figure 7c), indicating successful incorporation. Measurement of labeled HDAC4 in the presence of TFG ligand (Figure 7d) did not induce a shift in the tfmPhe746 signal at -62.3 .

The absence of difference in chemical shift upon incubation with the TFG ligand indicates no significant changes in the local environment of the tfmPhe746 label, suggesting no conformational changes of HDAC4 and is contrary to expected results based on the corresponding crystal structures of apo HDAC4 and HDAC4 in complex with the TFG ligand. This points to the unlikeness of the TFG ligand to induce the open conformation and puts the existence of the open conformation in solution into question. As a result, the open conformation might not be relevant to the biological function of the protein and is more likely to be an artificial conformation state under perhaps non-native conditions.

3 | CONCLUSIONS

Some crystal structures show an open conformation of HDAC4 in complex with several ligands, in particular the TFG ligand. This observation raised the possibility of developing isozyme-specific inhibitors targeting this

specific conformation, in light of the fact that the highly conserved binding pocket in the active site of the HDAC protein family poses a major challenge. In this study, we elucidate the potential importance of the open conformation under physiological conditions in solution. An HDAC4 double mutant variant lacking zinc ion binding in the sZBD showed a dramatic decrease in enzyme activity, in agreement with previous results. In addition, the local mutations in the sZBD showed a dramatic effect on the global structural integrity and stability of the protein, resulting in a highly disordered structure of HDAC4 in solution, which is clearly inconsistent with the reported open conformation. The ratio of α -helices to β -sheets changed significantly, and native IM-MS revealed a highly disordered conformational state of HDAC4 with larger segments lacking folded secondary structures, in agreement with thermal stability measurements. This further demonstrated that small changes in one region of a protein can have dramatic effects on distant regions or, as in our case, even on the global structure of HDAC4 protein. Native MS and NMR were used to elucidate the effects of ligand binding on the conformation of HDAC4 in solution. None of the ligands, including the TFG ligand, induced a conformational change comparable to the open conformation in solution. In summary, the open conformation of HDAC4 is not detectable in solution using different complementary biophysical methods. Therefore, we conclude this conformation does not seem to be relevant in a biological context and cannot be used for the development of isozyme-specific HDAC4 inhibitors.

4 | MATERIALS AND METHODS

4.1 | Mutagenesis and recombinant protein production

All HDAC4 constructs were the C-terminal domain of human HDAC4 (T648–T1057) and were produced in *Escherichia coli* BL21(DE) using a pET14b vector system containing the HDAC4 gene fused to a His6-SUMO tag. For the HDAC4 wild type, overnight cultures in Lennox LB media (20 g/L) and 100 µg/mL ampicillin were incubated under shaking at 37°C. The next day flasks containing sterile auto-induction media (3.08 g/L KH₂PO₄, 3.10 g/L Na₂HPO₄, 0.44 g/L MgSO₄, and 20 g/L Lennox LB media), 4.6 g/L glycerol, 0.45 g/L glucose, 1.2 g/L lactose, and 100 µg/mL ampicillin were inoculated with overnight culture and incubated at 30°C overnight under shaking. The next day cells were harvested by centrifugation (6–16 K centrifuge, Sigma, Osterode am Harz, Germany) at 3000g (4°C) for 10 min and frozen (–20°C) for storage. On the first day of protein purification the frozen cell pellet was thawed and resuspended in IMAC Buffer A (150 mM KCl, 50 mM TRIS–HCl, pH 8.0) and 3 µg/mL DNase I (AppliChem, Darmsadt, Germany), 5 mM dithiothreitol (AppliChem, Darmsadt, Germany) and 0.1 mg/mL lysozyme (Roth, Karlsruhe, Germany) were added. The cell suspension was cooled in an ice bath and stirred during cell lysis via ultrasound (Digital Sonofier C25, Branson, MO, USA). Subsequently, cell debris were removed by centrifugation at 18,000g at 4°C for 30 min (6–16 K centrifuge, Sigma, Osterode am Harz, Germany). The sample was filtered with a 0.45 µm filter (Filtropur, Sarstedt, Nümbrecht, Germany), diluted to 100 mL and 5 mM imidazole was added. The IMAC column (5 mL cComplete His-Tag Purification Resin, Roche, Basel, Switzerland) was washed with 3 CV (column volume) water to remove the 20% ethanol for storing conditions and was equilibrated with 10 CV of IMAC-Buffer A containing 5 mM imidazole. The column was loaded with the sample and subsequently washed with 5 CV IMAC-Buffer A containing 5 mM imidazole. Elution was carried out IMAC Buffer A containing 75 mM of imidazole (step elution). Protein-containing fractions were pooled, diluted to 50 mL and 6 µg/mL SUMO protease and 5 mM dithiothreitol were added. The sample was dialyzed at 4°C overnight against 2 L IMAC-Buffer A containing 5 mM dithiothreitol to remove imidazole using a dialysis tube (Membra-Cel Dialysis Tubing (MWCO 3500 Da), Serva, Heidelberg, Germany). The next day hydrophobic interaction chromatography (HIC) was performed to remove the His6-SUMO tag. After washing the column (HiTrap Phenyl HP, Cytiva, Freiburg, Germany) with 3 CV to remove

the 20% ethanol for storing conditions and was equilibrated with 3 CV of HIC-Buffer B (50 mM TRIS–HCl, pH 8.0) followed by 10 CV HIC-Buffer A (1 M (NH₄)₂SO₄, 50 mM TRIS–HCl, pH 8.0). After filtering the sample with a 0.2 µm filter (Filtropur, Sarstedt, Nümbrecht, Germany) and diluted with 50 mL of 2× HIC-Buffer A, it was loaded onto the HIC column. Subsequently, the column was washed with 5 CV HIC-Buffer A and the protein was eluted with HIC-Buffer B (step elution). The protein-containing fractions were concentrated by ultrafiltration (Vivaspin 2, MWCO 30 kDa, Sartorius, Goettingen, Germany) at 8000 g and 4°C (3–30KS centrifuge, Sigma, Osterode am Harz, Germany) to ca. 2 mL, 5 mM dithiothreitol was added and the sample was stored at 4°C. The next day, the final purification step (size exclusion chromatography) was performed. The SEC-column (HiLoad Superdex 16/600 75 µg column, Cytiva, Freiburg, Germany) was washed with 1.5 CV water to remove the 20% ethanol for storing conditions and equilibrated with 3 CV SEC-Buffer (150 mM KCl, 50 mM TRIS–HCl, 1 mM TCEP, 5% glycerol, pH 8.0). Subsequently, SEC was performed and protein-containing fractions were concentrated via ultracentrifugation (see above), freezed in liquid nitrogen, and stored at –80°C. All chromatography steps were performed using an Äkta Pure chromatography system (GE Healthcare Life Sciences, Freiburg, Germany). Flow rates were 5 mL/min for IMAC and HIC and 1 mL/min for SEC. All column CIP protocols were performed as recommended by the respective manufacturer.

For the ¹⁵N labeled and ncAA incorporated HDAC4 samples the basic procedure was the same but M9 minimal media instead of LB media and auto-induction media was used for ¹⁵N labeling. The composition of the M9 minimal media is provided in Table S9. After transferring the overnight culture in production flasks the cultures were incubated at 30°C under shaking and protein production was induced at an OD₆₀₀ of 0.7 with 400 µM IPTG (Roth, Karlsruhe, Germany). For the incorporation of the ncAA (tfmF) the pDule-tfmF A65V S158A suppressor plasmid and the ncAA was purchased from Addgene (85484) and BLDpharm (Kaiserslautern, Germany), respectively. Cells were incubated in LB media at 37°C up to an OD₆₀₀ of 0.7. The ncAA was dispersed in sterile water, and a small amount of NaOH was added to ensure complete dissolution. It was added to the medium 45 min prior to induction with a final concentration of 1 mM. Induction was performed with 400 µM of IPTG and 0.02% arabinose (Roth, Karlsruhe, Germany). After induction, the cells were incubated at 30°C overnight.

HDAC4 variants (Cys669Ala/His675Ala double mutant and stop codon (TAG) mutant at position

Phe764) were generated by splicing by overlap extension polymerase chain reaction (PCR; Higuchi et al., 1988). Sequences of respective primers are provided in Table S10.

4.2 | Molecular docking

Preparation, visualization of structural data, and molecular docking were performed using MOE 2022.02 software (Chemical Computing Group ULC, Canada). The crystal structures of the closed (PDB-ID: 4CBY) and open conformation of HDAC4 (PDB-ID: 2VQJ) were obtained from RCSB Protein Data Bank. The structure files were loaded into the program, water molecules were removed, and the partial charges of all protein and ligand atoms were calculated using the implemented Amber14 force field. Subsequently, the protein was protonated using the implemented Protonate-3D procedure for a temperature of 300 K, pH 7, and 0.1 M salt. All atoms were computational titrated and allowed to flip during the calculation. The Generalized Born/Volume Integral (GB/VI) formalism was applied to calculate the electrostatics. The dielectric constants used for the protein and the solvent were 2 and 80, respectively. To simulate the repulsive part of the van der Waals energy, the 800R3 setting of the Protonate-3D procedure was chosen, while using a cutoff distance of 10 Å, above which van der Waals interactions between two atoms would be ignored. Molecular docking was performed using the Induced Fit protocol, which includes the protein sidechains in the refinement stage. The triangle matcher was chosen for placement of the ligand in the binding site, and resulting binding poses were ranked with the London dG scoring function. The best 50 poses were passed to the refinement and energy minimization in the pocket using the induced fit method and then rescored with the GB/VI/WSA dG scoring function. The docking procedure was validated by redocking of the cocrystallized ligand in the respective receptor protein. The resulting binding pose showed broad consistency with an RMSD-value of 0.76 Å for the overall hydroxamic acid ligand in the closed conformation of HDAC4 (PDB-ID 4CBY). The position of the hydroxamate warhead and adjacent atoms was even better defined with an RMSD-value of 0.26 Å (Figure S4).

4.3 | HDAC4 activity assay

Enzyme activity tests were performed with 1 nM of HDAC4 wild type and 10 nM of the double mutant (Cys669Ala/His675Ala) and 20 μM Boc-Lys(Ffa)-7-Amino-4-methylcoumarin (Bachem, Bubendorf, Switzerland) and

carried out in a black 96 well half area microtiter plate (Greiner, Kremsmünster, Austria) for 1 h at 30°C in Assay-Buffer (25 mM Tris-HCl, 75 mM KCl, 0.00001% Pluronic, pH 8.0) under shaking. The reaction was terminated by the addition of 1.7 μM SATFMK. To release the 7-amino-4-methyl-coumarin fluorophore (AMC) from the deacetylated substrate, 0.4 mg/mL trypsin was added, followed by another incubation step for 1 h at 30°C under shaking. The assay is based on the work of Wegener et al. (2003). Fluorescence intensity was measured in a PheraStar Plus (BMG Labtech, Ortenberg, Germany) fluorescence plate reader at 450 nm (Ex: 350 nm) and the blank (substrate in assay buffer without HDAC4) was subtracted from the signal. Subsequently, fluorescence intensity was converted to turned over substrate using a calibration curve. Finally, the turned over substrate was divided by the respective HDAC4 concentration for fair enzyme activity comparison.

4.4 | Thermal shift assay

Assays for determining thermal stability and thermal stabilization were performed in a Quant Studio 5 real-time qPCR device (Thermo Fisher Scientific, Darmstadt, Germany) with SYPRO orange (Sigma-Aldrich, Taufkirchen, Germany) as fluorescence dye. The samples contained 11 μM of protein and 10-fold SYPRO orange in assay buffer. All samples were incubated for 1 h at 30°C in the qPCR device to ensure chemical equilibrium. Afterwards, the heat gradient was initiated (0.015°C/s) and changes in fluorescence were measured in the qPCR device's TAMRA channel (623 nm [Ex = 580 nm]) and plotted against temperature. The increase in fluorescence during the thermal stability assay is attributed to the fluorescent dye, which increases its intensity upon binding to hydrophobic regions of a protein. By increasing the sample temperature, the protein unfolds and its hydrophobicity increases, which can be quantified by the increase in fluorescence. In order to determine melting curves, the first derivative of the fluorescence signal was calculated and plotted against temperature, the point of inflection indicated the melting point of the respective sample. Calculations were performed in protein thermal shift software (Thermo Fisher Scientific, Darmstadt, Germany). Measurements were performed in quadruples ($n = 4$).

4.5 | CD spectroscopy

CD spectra were obtained using a Jasco J-1500 CD spectrometer (Jasco, Pfungstadt, Germany) with protein sample concentration of 5 μM in CD-Buffer (5 mM Tris-HCl,

15 mM KCl, pH 8.0) at a temperature of 20°C in a quartz cuvette with 1 mm path length. The measurements were performed with a bandwidth of 4 nm and a scanning speed of 50 nm/min. Each sample underwent 10 scans, which were then averaged. According to the manufacturer, the voltage of the photomultiplier tube (PMT) should not exceed 700 V for a reliable CD signal. This was the case between 192 and 260 nm in our measurements. For data processing, the buffer signal was subtracted, the acquired data were baseline corrected and transformed into mean residue molar ellipticity (expressed in $\text{deg cm}^2 \text{dmol}^{-1}$) using CDToolX software (<https://cdtools.cryst.bbk.ac.uk/>). The analysis and evaluation of the CD data were conducted using the online tools provided by BeStSel (<https://bestsel.elte.hu/>), which employ algorithms developed by Micsonai et al. (2015, 2018).

4.6 | ^{19}F -NMR measurements

Measurements were performed on an AV 500 NMR spectrometer (Bruker, MA, USA), equipped with a broadband probe and operating at 470.6 MHz for fluorine. Measurements of the complex between fluorinated protein and TFG ligand were conducted at 21°C in shigemini nmr tubes; free fluorinated protein was measured at 25°C. Samples were prepared in stated concentrations using labeled protein (200 μM), 500 μM TFG ligand in NMR buffer (50 mM HEPES, 150 mM KCl, 1 mM TCEP, pH 7.5) in $\text{D}_2\text{O}/\text{H}_2\text{O}$ (250 μL).

4.7 | IM-MS simulations and measurements

IM-MS is a technique for determining the CCS of analytes in the gas phase (Gabelica & Marklund, 2018). This is not limited to small molecules but also includes native proteins and unfolding observation (Ruotolo et al., 2007).

Using the crystal structures of HDAC4 wild type (PDB-ID: 4CBY, closed conformation) and the crystal structure of HDAC4 wild type with bound TFG ligand (PDB-ID: 2VQJ, open conformation), theoretical CCS values were calculated. For this purpose, we used IMPACT software (Oxford University Innovation Limited, Oxford, Great Britain), which calculates a CCS-value based on the crystal structure and the projection approximation (PA; Mack Jr., 1925) and finally a CCS-value by the trajectory method (TJM) using a correlation (Marklund et al., 2015). The ligands of the crystal structures were included in the calculation. Default settings were used.

Note that the IMPACT software computes theoretical CCS values using helium as drift gas, whereas the actual measurements employed nitrogen as drift gas. Generally, the use of nitrogen as a drift gas results in larger CCS values in comparison to helium, due to nitrogen's polarizability, which can lead to interactions with charges on the protein's surface. Consequently, this interaction can result in extended drift times and subsequently larger CCS values. We used a regression analysis based on reference CCS values obtained with both helium and nitrogen as drift gases. The charge states and literature CCS used for the calibrants are listed in Table S11. A logarithmic regression model was chosen for calibration (Ruotolo et al., 2008). The regression values are listed in Figure S12. The CCS-value for nitrogen as drift gas, calculated using the TJM method, can be estimated to be 3910 \AA^2 for the open conformation of HDAC4. The estimated CCS-value using helium as the drift gas was smaller (3481 \AA^2). Therefore, we expected an even larger increase (compared with Figure 4) in CCS values between the two conformations.

During IM-MS measurements, proteins are in a balance between the Coulomb repulsion, which can cause the protein to increase in size to the point of unfolding, and intramolecular interactions, which keep the protein in a compact conformation (Zhong et al., 2014). Thus, with each additional charge, some increase in CCS values can be expected as the Coulomb repulsion increases, but proteins with pronounced secondary structures exhibit more modest increases of CCS values (e.g., for HDAC4 and its complexes with different ligands) compared with proteins with less defined or disturbed secondary structures (e.g., HDAC4 Cys669Ala/His675Ala variant). At higher charge states this effect becomes more severe.

For the IM-MS measurements, water (LC-MS grade) was purchased from Fisher Scientific, Hempton, USA. The acetonitrile (LC-MS grade) and formic acid (p.a.) were purchased from Merck, Darmstadt, Germany. For the 200 mM ammonium acetate solution a 7.5 M ammonium acetate stock solution from Merck, Darmstadt, Germany, was diluted with water. Tris(2-carboxyethyl) phosphine hydrochloride (TCEP) and dimethyl sulfoxide (DMSO) were purchased from Carl Roth, Karlsruhe, Germany. Horse holo-myoglobin and bovine serum albumin (BSA) for CCS calibration were purchased from Merck, Darmstadt, Germany. The Synapt XS was calibrated with sodium iodide solution from Waters, Milford, USA. For IM-MS measurement, the protein samples were rebuffed with 500 μL Amicon Ultra Filter from Merck, Darmstadt, Germany, with a 10 K cutoff at 14,000g for 15 min with 200 mM ammonia acetate and 0.5 mM TCEP four times. Immediately prior to measurement, additional rebuffing with 200 mM ammonium acetate

was performed. The protein solution was then diluted with 200 mM ammonium acetate to the final concentration of 20 μ M. The ligands in DMSO were diluted with 200 mM ammonium acetate to a final concentration of 30 μ M. The apo-HDAC4 WT contained 0.6 vol% DMSO as a negative control. The samples were measured with direct-infusion nanoESI at a Synapt XS with traveling wave technology from Waters (Milford, USA; Pringle et al., 2007). For this, 10 μ L protein solution was loaded in a self-pulled nanoESI capillary. A micropipette puller Model P-97 from Sutter Instrument, Novato, USA, was used to make the capillaries. The Capillary Voltage was between 1.0 and 1.7 kV, Sampling Cone 30 V, Source Offset 20 V, Source Temperature 30°C, Cone Gas Flow 100 L/h, and Purge Gas Flow 550 mL/h for the nanoESI source. For mass recalibration, we performed an internal calibration using the masses of the analytes with a first order regression. For the IM-MS measurements, we used helium at 180 mL/min as the cooling gas and nitrogen at 90 mL/min as the drift gas. For the traveling wave, different wave velocities of 800, 900, and 1000 m/s were used. The wave height was kept at 40 V, and the transfer cell wave velocity and height were constant at 140 m/s and 4 V, respectively. The Trap DC bias voltage was 28 V. The quadrupole with the RF generator of 300 kHz was set to RF only, and the time-of-flight (TOF) was in resolution mode. The mass range was from 400 to 5000 m/z . Before the measurements, the MS was mass calibrated with sodium iodide to 5000 m/z . For CCS calibration, we measured horse holo-myoglobin and BSA with the same settings.

AUTHOR CONTRIBUTIONS

Markus Schweipert: Investigation; methodology; writing—review and editing; writing—original draft; visualization; formal analysis. **Thomas Nehls:** Investigation; methodology; writing—review and editing; visualization; formal analysis. **Anton Frühauf:** Investigation; methodology; formal analysis; visualization. **Cecilé Debarnot:** Investigation; formal analysis. **Adarsh Kumar:** Methodology; writing—review and editing; visualization; formal analysis; validation. **Stefan Knapp:** Methodology; writing—review and editing; supervision; funding acquisition; formal analysis; validation. **Frederik Lermyte:** Supervision; writing—review and editing; validation; methodology; funding acquisition; formal analysis. **Franz-Josef Meyer-Almes:** Conceptualization; funding acquisition; writing—original draft; validation; visualization; investigation; writing—review and editing; formal analysis; project administration; supervision.

ACKNOWLEDGMENT

Open Access funding enabled and organized by Projekt DEAL.

FUNDING INFORMATION

This research was supported by the LOEWE priority program TRABITA, State of Hesse, Germany (to FJMA, FL, SK, MS, and TN). The Synapt XS instrument was funded through the German Research Foundation (DFG), grant number (461372424).

ORCID

Franz-Josef Meyer-Almes  <https://orcid.org/0000-0002-1001-3249>

REFERENCES

- Asfaha Y, Schrenk C, Alves Avelar LA, Hamacher A, Pflieger M, Kassack MU, et al. Recent advances in class IIa histone deacetylases research. *Bioorg Med Chem*. 2019;27:115087.
- Bondarev AD, Attwood MM, Jonsson J, Chubarev VN, Tarasov VV, Schioth HB. Recent developments of HDAC inhibitors: emerging indications and novel molecules. *Br J Clin Pharmacol*. 2021;87:4577–97.
- Bottomley MJ, Lo Surdo P, Di Giovine P, Cirillo A, Scarpelli R, Ferrigno F, et al. Structural and functional analysis of the human HDAC4 catalytic domain reveals a regulatory structural zinc-binding domain. *J Biol Chem*. 2008;283:26694–704.
- Bradley D. The evolution of post-translational modifications. *Curr Opin Genet Dev*. 2022;76:101956.
- Breuker K, McLafferty FW. Stepwise evolution of protein native structure with electrospray into the gas phase, 10(–12) to 10(2) s. *Proc Natl Acad Sci U S A*. 2008;105:18145–52.
- Burli RW, Luckhurst CA, Aziz O, Matthews KL, Yates D, Lyons KA, et al. Design, synthesis, and biological evaluation of potent and selective class IIa histone deacetylase (HDAC) inhibitors as a potential therapy for Huntington's disease. *J Med Chem*. 2013;56:9934–54.
- Chen H, Viel S, Ziarelli F, Peng L. 19F NMR: a valuable tool for studying biological events. *Chem Soc Rev*. 2013;42:7971–82.
- Clocchiatti A, Florean C, Brancolini C. Class IIa HDACs: from important roles in differentiation to possible implications in tumorigenesis. *J Cell Mol Med*. 2011;15:1833–46.
- Di Giorgio E, Gagliostro E, Brancolini C. Selective class IIa HDAC inhibitors: myth or reality. *Cell Mol Life Sci*. 2015;72:73–86.
- Dowling DP, Gattis SG, Fierke CA, Christianson DW. Structures of metal-substituted human histone deacetylase 8 provide mechanistic inferences on biological function. *Biochemistry*. 2010;49:5048–56.
- Federspiel JD, Greco TM, Lum KK, Cristea IM. Hdac4 interactions in Huntington's disease viewed through the prism of multiomics. *Mol Cell Proteomics*. 2019;18:S92–S113.
- Fischle W, Kiermer V, Dequiedt F, Verdin E. The emerging role of class II histone deacetylases. *Biochem Cell Biol*. 2001;79:337–48.
- Gabelica V, Marklund E. Fundamentals of ion mobility spectrometry. *Curr Opin Chem Biol*. 2018;42:51–9.
- Gantt SL, Gattis SG, Fierke CA. Catalytic activity and inhibition of human histone deacetylase 8 is dependent on the identity of the active site metal ion. *Biochemistry*. 2006;45:6170–8.
- Goddard TD, Huang CC, Meng EC, Pettersen EF, Couch GS, Morris JH, et al. UCSF ChimeraX: meeting modern challenges in visualization and analysis. *Protein Sci*. 2018;27:14–25.
- Greenfield NJ. Using circular dichroism spectra to estimate protein secondary structure. *Nat Protoc*. 2006;1:2876–90.

- Gronenborn AM. Small, but powerful and attractive: (19)F in biomolecular NMR. *Structure*. 2022;30:6–14. PMID: 34995480 [Medline].
- Higuchi R, Krummel B, Saiki RK. A general method of in vitro preparation and specific mutagenesis of DNA fragments: study of protein and DNA interactions. *Nucleic Acids Res*. 1988;16:7351–67.
- Ho TCS, Chan AHY, Ganesan A. Thirty years of HDAC inhibitors: 2020 insight and hindsight. *J Med Chem*. 2020;63:12460–84.
- Jackson JC, Hammill JT, Mehl RA. Site-specific incorporation of a 19F-amino acid into proteins as an NMR probe for characterizing protein structure and reactivity. *J Am Chem Soc*. 2007;129:1160–6.
- Kitevski-LeBlanc JL, Prosser RS. Current applications of 19F NMR to studies of protein structure and dynamics. *Prog Nucl Magn Reson Spectrosc*. 2012;62:1–33.
- Mack E Jr. Average cross-sectional areas of molecules by gaseous diffusion methods. *J Am Chem Soc*. 1925;47:2468–82.
- Marklund EG, Degiacomi MT, Robinson CV, Baldwin AJ, Benesch JL. Collision cross sections for structural proteomics. *Structure*. 2015;23:791–9.
- Micsonai A, Wien F, Bulyáki É, Kun J, Moussong É, Lee YH, et al. BeStSel: a web server for accurate protein secondary structure prediction and fold recognition from the circular dichroism spectra. *Nucleic Acids Res*. 2018;46:W315–22.
- Micsonai A, Wien F, Kernya L, Lee Y-H, Goto Y, Réfrégiers M, et al. Accurate secondary structure prediction and fold recognition for circular dichroism spectroscopy. *Proc Natl Acad Sci U S A*. 2015;112:E3095–103.
- Mielcarek M, Landles C, Weiss A, Bradaia A, Seredenina T, Inuabasi L, et al. HDAC4 reduction: a novel therapeutic strategy to target cytoplasmic huntingtin and ameliorate neurodegeneration. *PLoS Biol*. 2013;11:e1001717.
- Mielcarek M, Zielonka D, Carnemolla A, Marcinkowski JT, Guidez F. HDAC4 as a potential therapeutic target in neurodegenerative diseases: a summary of recent achievements. *Front Cell Neurosci*. 2015;9:42.
- Mirts EN, Bhagi-Damodaran A, Lu Y. Understanding and modulating metalloenzymes with unnatural amino acids, non-native metal ions, and non-native metal cofactors. *Acc Chem Res*. 2019;52:935–44.
- Pringle SD, Giles K, Wildgoose JL, Williams JP, Slade SE, Thalassinou K, et al. An investigation of the mobility separation of some peptide and protein ions using a new hybrid quadrupole/travelling wave IMS/oa-ToF instrument. *Int J Mass Spectrom*. 2007;261:1–12.
- Ruotolo BT, Benesch JL, Sandercock AM, Hyung SJ, Robinson CV. Ion mobility-mass spectrometry analysis of large protein complexes. *Nat Protoc*. 2008;3:1139–52.
- Ruotolo BT, Hyung SJ, Robinson PM, Giles K, Bateman RH, Robinson CV. Ion mobility-mass spectrometry reveals long-lived, unfolded intermediates in the dissociation of protein complexes. *Angew Chem Int ed Engl*. 2007;46:8001–4.
- Schweipert M, Jänsch N, Upadhyay N, Tilekar K, Wozny E, Basheer S, et al. Mechanistic insights into binding of ligands with thiazolidinedione warhead to human histone deacetylase 4. *Pharmaceuticals*. 2021;14:1032. <https://doi.org/10.3390/ph14101032>
- Shen Z, Bei Y, Lin H, Wei T, Dai Y, Hu Y, et al. The role of class IIa histone deacetylases in regulating endothelial function. *Front Physiol*. 2023;14:1091794.
- Turzo SMBA, Seffernick JT, Lyskov S, Lindert S. Predicting ion mobility collision cross sections using projection approximation with ROSIE-PARCS webserver. *Brief Bioinform*. 2023;24:bbad308.
- Wang X, Liu J, Zhen J, Zhang C, Wan Q, Liu G, et al. Histone deacetylase 4 selectively contributes to podocyte injury in diabetic nephropathy. *Kidney Int*. 2014;86:712–25.
- Wang Z, Qin G, Zhao TC. HDAC4: mechanism of regulation and biological functions. *Epigenomics*. 2014;6:139–50.
- Wegener D, Wirsching F, Riestler D, Schwienhorst A. A fluorogenic histone deacetylase assay well suited for high-throughput activity screening. *Chem Biol*. 2003;10:61–8.
- Witt O, Deubzer HE, Milde T, Oehme I. HDAC family: what are the cancer relevant targets? *Cancer Lett*. 2009;277:8–21.
- Yang F, Zhao N, Ge D, Chen Y. Next-generation of selective histone deacetylase inhibitors. *RSC Adv*. 2019;9:19571–83.
- Ye L, Larda ST, Frank Li YF, Manglik A, Prosser RS. A comparison of chemical shift sensitivity of trifluoromethyl tags: optimizing resolution in ¹⁹F NMR studies of proteins. *J Biomol NMR*. 2015;62:97–103.
- Zhong Y, Han L, Ruotolo BT. Collisional and coulombic unfolding of gas-phase proteins: high correlation to their domain structures in solution. *Angew Chem*. 2014;126:9363–6.

SUPPORTING INFORMATION

Additional supporting information can be found online in the Supporting Information section at the end of this article.

How to cite this article: Schweipert M, Nehls T, Frühauf A, Debarnot C, Kumar A, Knapp S, et al. The catalytic domain of free or ligand bound histone deacetylase 4 occurs in solution predominantly in closed conformation. *Protein Science*. 2024;33(3):e4917. <https://doi.org/10.1002/pro.4917>